ACS APPLIED MATERIALS & INTERFACES

Research Article

www.acsami.org

Fluorescent Detection of Lead in Environmental Water and Urine Samples Using Enzyme Mimics of Catechin-Synthesized Au Nanoparticles

Yan-Shiuan Wu, Fan-Feng Huang, and Yang-Wei Lin*

Department of Chemistry, National Changhua University of Education, Changhua, Taiwan

Supporting Information

ABSTRACT: A facile, cost-effective, and sensitive fluorescent method for Pb^{2+} ion detection had been developed using catechin synthesized gold nanoparticles (C−Au NPs). The Pb−catechin complexes and Pb−Au alloys that formed on the C−Au NPs surfaces allowed NPs to exhibit peroxidase-mimicking catalytic activity in the H_2O_2-mediated oxidation of Amplex UltraRed (AUR). In 5 mM Tris-acetate buffers at pH 7.0, the H_2O_2−AUR−C−Au NP probe was highly selective (>100-fold) for Pb^{2+} ions in the presence of other tested metal ions (K^+, Ag^+, Na^+, Cd^{2+}, Ni^{2+}, Ca^{2+}, Hg^{2+}, Sr^{2+}, Co^{2+}, Cu^{2+}, Ba^{2+}, Fe^{2+}, Mg^{2+}, Cr^{3+}, and Fe^{3+} ions). The fluorescence intensity (excitation/emission maxima ~540/588 nm) of the AUR product was proportional to the concentration of Pb^{2+} ions in the range of 10 nM−1.0 μM with a linear correlation (R^2 = 0.99). The H_2O_2−AUR−C−Au NP probe detected Pb^{2+} ions with a limit of detection (signal-to-noise ratio: 3) of 1.5 nM. The practicality of the H_2O_2−AUR−C−Au NP probe was validated for the determination of Pb^{2+} ion concentration in environmental water and urine samples, demonstrating its advantages of simplicity, selectivity, and sensitivity.

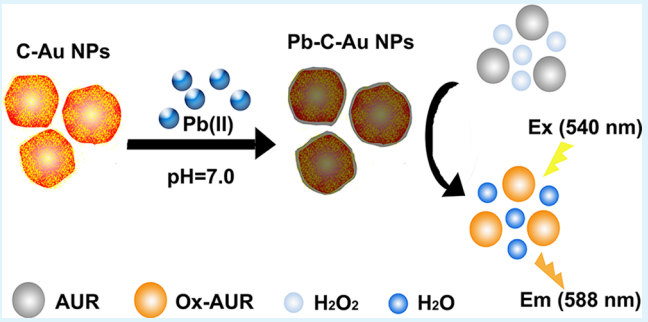

KEYWORDS: *Amplex UltraRed, catechin, lead(II), environmental water samples, urine sample*

INTRODUCTION

Lead (Pb) has attracted much attention because it plays an important role in biological, environmental, and chemical fields.[1,2] It has been reported that Pb^{2+} ions cause oxidative stress by inducing the generation of reactive oxygen species and reducing the antioxidant defense system of cells, suggesting that antioxidants can play an important role in the treatment of Pb poisoning.[3−6] Exposure to Pb has been associated with behavioral abnormalities, learning impairment, decreased hearing, and impaired cognitive functions in humans and experimental animals.[7] Therefore, the U.S. Food and Drug Administration suggests an action level for Pb of 2.5 μM (518 μgL^{-1}) in products intended for children.[8] Hence, it is particularly important to develop a sensitive, selective, and reliable analytical technique for Pb determination.

During the past decade, many DNA-based fluorescent sensors are developed for monitoring a low level of Pb^{2+} ions because of their sensitivity, facility, and rapidness.[9−19] For example, Lin and co-workers used polyguanine (G_{33})/terbium ion (Tb^{3+}) conjugates for the detection of Pb^{2+} ions.[13] Because Pb^{2+} ions compete with Tb^{3+} ions to form complexes with G_{33}, the extent of formation of the G_{33}−Tb^{3+} complexes decreases with increasing Pb^{2+} concentration, leading to decreased fluorescence at 545 nm when excited at 290 nm. However, this detection system is mostly not practical because Pb^{2+} ions induced a "turn off" sensing mechanism. DNAzyme-based sensors have been demonstrated for the detection of Pb^{2+} ions through their induced changes in the catalytic activity of DNAzymes.[20] DNAzymes are non-natural short-stranded nucleic acids that act much like enzymes, catalyzing many biochemical reactions. For example, Li and co-workers developed a fluorescence approach for the highly selective and sensitive detection of Pb^{2+} ions using AGRO100, a G-quadruplex DNAzyme.[14] This sensing strategy is based on Pb^{2+} ions inducing the increased DNAzyme activity of AGRO100 in the presence of hemin, which acts as a cofactor for catalyzing the H_2O_2-mediated oxidation of Amplex UltraRed (AUR). For 5 mM Tris-acetate buffers at pH 7.4 in the presence of 100 mM NaCl, the AGRO100-AUR probe detects Pb^{2+} ions with a limit of detection (S/N ratio of 3) of 1.0 nM. However, the reaction time requires 2 h because of low catalytic efficiency of the AGRO100-AUR probe.

Gold nanoparticles (Au NPs) possess distinct physical and chemical attributes that make them excellent scaffolds for the fabrication of novel chemical and biological sensors.[21] In the past decade of research, the advent of Au NP as a sensory element provides us a broad spectrum of innovative approaches for the detection of heavy metal ions.[22−24] Many colorimetric

Received: December 10, 2012
Accepted: January 31, 2013
Published: January 31, 2013

   dx.doi.org/10.1021/am3030454 | ACS Appl. Mater. Interfaces 2013, 5, 1503−1509

detection methods for Pb^{2+} ions using DNA-functionalized Au NPs have also been reported.[25−27] For example, Lu and co-workers developed a series of functional DNAzyme-based sensors using Au NPs.[28] The detection range of the sensor could be turned from 3 nM to 1 μM. Dong and co-workers reported a DNAzyme-based colorimetric sensor for Pb^{2+} with a detection limit of 500 nM.[29] However, synthesis of DNA oligomers and their chemical modification with Au NPs are complex and expensive. In addition, colorimetric techniques generally display higher detection limits. Recently, Chang and co-workers reported a fluorescence assay for the sensitive and selective detection of Hg^{2+} and Pb^{2+} ions using Au NP-based probe under different pH conditions.[30] The sensing strategy is based on Hg−Au and Pb−Au alloys formed on the Au NP surfaces allowing Au NPs to exhibit peroxidase-mimicking catalytic activity in the H_2O_2-mediated oxidation of AUR. The linear responses for Hg^{2+} and Pb^{2+} ions are both over ranges 0.05−1 μM (R^2 = 0.993) and 0.05−5 μM (R^2 = 0.996), respectively. In order to detect Pb^{2+} ions selectively and sensitively in real samples, the pretreatment process should be careful to avoid the matrix difference because it must be performed at the basic conditions. Thus, this may limit the practicality of the probe for the detection of Pb^{2+} ions in real samples.

Previously, we synthesized Au nanostructures from sodium tetrachloroaurate(III) dihydrate in tea infusions. Flavonoids, catechins, and various phytochemicals that are the main substituents of tea infusions possess electron-rich features such as hydroxyl groups that are responsible for the reduction of $AuCl_4^-$ ions and for the stabilization of the as-prepared Au nanostructures.[31,32] In particular, tea catechins are strong metal ion chelators because of their catechol structure, which has been shown to form stable complexes with metal ions.[33] In this study, we developed a novel, simple, and nonaggregated catechin synthesized Au NP (C−Au NP) probe for the sensitive and selective detection of Pb^{2+} ions, on the basis of the influence on the catalytic activity of C−Au NPs toward the H_2O_2-mediated oxidation of AUR. The effects of the morphology of C−Au NPs, and the conditions of buffer, as well as the concentrations of H_2O_2 and AUR on the selectivity and sensitivity of the H_2O_2−AUR−C−Au NP probe for the detection of Pb^{2+} ions were evaluated. The practicality of the H_2O_2−AUR−C−Au NP probe was then validated through the detection of Pb^{2+} ions in environmental water samples and a urine sample.

CHEMICALS AND METHODS

Chemicals. All chemicals used were of analytical grade or of the highest purity available. Sodium tetrachloroaurate(III) dihydrate ($NaAuCl_4·2H_2O$), (+)-catechin hydrate, Tris (base), acetic acid, $AgNO_3$, $Pb(NO_3)_2$, $Ni(NO_3)_2·6H_2O$, $Cr(NO_3)_3·9H_2O$, NaCl, $CaCl_2·2H_2O$, $Sr(NO_3)_2$,$BaCl_2·6H_2O$, $Cd(NO_3)_2·4H_2O$, $FeCl_2·4H_2O$, $Mg(NO_3)_2·6H_2O$, $FeCl_3$, $HgCl_2$, $Co(NO_3)_2·6H_2O$, $Cu(NO_3)_2·2.5H_2O$, and KCl were obtained from Sigma Aldrich (St. Louis, MO, USA). The AUR reagent was purchased from Invitrogen (Eugene, OR, USA). Milli-Q ultrapure water was used in all experiments.

Preparation of C−Au NPs. In a typical process for synthesis of C−Au NPs, $NaAuCl_4·2H_2O$ (10 mM, 2.0 mL) was mixed with Milli-Q water (50 mL) in the presence of different concentrations of catechin (0.05−1.4 mM). The mixture was stirred gently at 40 °C for 10 min, at which time the color changed from yellow to red, indicating the formation of C−Au NPs. After stirring for another 50 min, the mixture was purified via centrifugation (RCF 10 620*g*) for 10 min. The as-prepared C−Au NPs were then redispersed in 5 mL of ultrapure water. Herein, the concentration of the as-prepared C−Au NPs is ca. 0.24 nM.

Characterization of C−Au NPs. UV−vis absorption spectra of C−Au NPs were recorded using a Synergy H1 Hybrid Multi-Mode Microplate Reader (Biotek Instruments, Winooski, VT, USA). A JEOL-1200EX II (JEOL, Tokyo, Japan) TEM system was used to measure the size and shape of C−Au NPs. An energy-dispersive X-ray spectroscopy (EDS) system (Oxford Instruments, Oxfordshire, UK) was used to confirm the compositions of the prepared Au nanostructures. X-ray diffraction (XRD) measurements were performed using a LabX XRD-6000 X-ray diffractometer (SHIMADZU., Kyoto, Japan) with Cu Kα radiation (λ = 0.15418 nm). FT-IR spectra of C−Au NPs were taken at room temperature using an Agilent Cary 600 Series FT-IR (Agilent, California, USA). Mass spectrometry experiments were performed in the negative ion mode using a Microflex matrix-assisted laser desorption/ionization-time-of-flight mass spectrometer (Bruker Daltonics, Bremen, Germany). Aliquots (1.0 μL) of catechin or C−Au NPs were pipetted onto a stainless steel 96-well MALDI target and dried in air at room temperature for 1 h prior to collecting surface-assisted laser desorption/ionization mass spectrometry (SALDI-MS) measurements. The hydrodynamic diameter and zeta potentials of C−Au NPs were measured using a Zetasizer Nano ZS90 apparatus (Malvern Instruments Ltd., Worcestershire, UK).

General Procedure for Fluorescence Analysis. Most of the metal salts used in this study were nitrate-based anions. Thus, a stock solution of metal ions (0.1 M) was prepared in 0.1 M HNO_3 and then diluted to 0−100 μM in ultrapure water. For selective determination of Pb^{2+} ions, separate aliquots of metal ion solutions (50 μL) were added to 5 mM Tris-acetate buffer (pH 7.0) solutions containing 0.24 nM C−Au NPs prepared using 0.2 mM catechin, 20 μM AUR, and 400 μM hydrogen peroxide to give final volumes of 500 μL. After equilibration at ambient temperature for 60 min, the mixtures were transferred separately into 96-well microtiter plates, and their fluorescence spectra were recorded using a Synergy H1 Hybrid Multi-Mode Microplate Reader. Determinations were performed in triplicate for three preparations of the samples.

Procedure for Pb Determination in Real Samples Using Atomic Absorption Spectroscopy. Lake and pond water samples were collected from the campus in National Changhua University of Education, Taiwan. Urine samples were collected from a healthy female. After the real samples were filtered through a 0.2 μm membrane, aliquots of the real samples (100 μL) were spiked with a standard solution of Pb^{2+} ions at the desired concentrations. The spiked samples were then diluted to 500 μL using a solution containing 0.24 nM C−Au NPs prepared using 0.2 mM catechin, 20 μM AUR, 600 μM hydrogen peroxide, and 5 mM Tris-acetate buffer at pH 7.0. The spiked samples were analyzed separately using the developed method and an atomic absorption spectrophotometric (AAS) method (Sens AA Atomic Absorption Spectrometer, GBC scientific equipment, Braeside VIC, Australia). Determinations were performed in triplicate for three preparations of the real samples.

RESULTS AND DISCUSSION

Characterization of C−Au NPs. At a constant concentration of $NaAuCl_4$ (0.4 mM), C−Au NPs were synthesized under various concentrations (0.05 to 1.4 mM) of catechin (Figure S1A, Supporting Information). It was observed that, as the concentration of catechin increased from 0.05 to 0.2 mM, the main SPR band blue-shifted, and became narrower and more intense. In addition, at higher concentrations of catechin (from 0.6 to 1.4 mM), the absorption band for Au produced a small shoulder at 535 nm. Such changes in the absorption response can be easily justified in terms of the morphology of the particles. TEM characterizations revealed that higher concentrations of catechin resulted in forming smaller particles and irregular shapes (Figure S1B, Supporting Information). It

Scheme 1. Cartoon Representation of the Fluorescent Sensing of Pb^{2+} Ions Based on the Pb^{2+} Ions Increasing the Catalytic Activity of C−Au NPs toward the H_2O_2-Mediated Oxidation of AUR

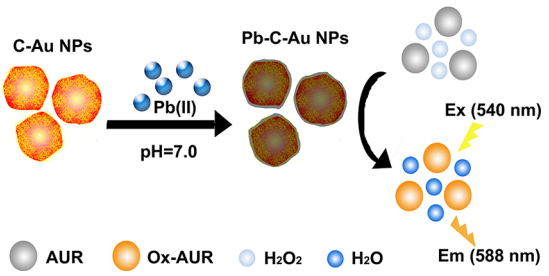

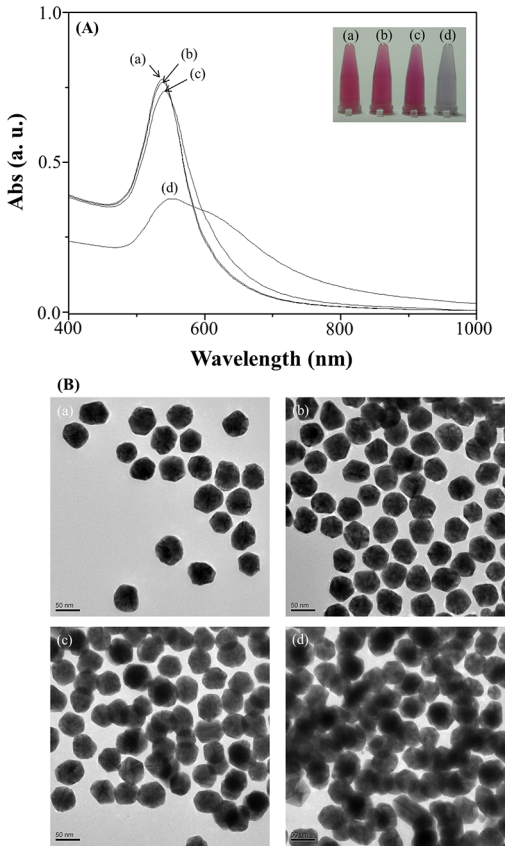

Figure 1. UV−vis absorbance spectra (A) and TEM images (B, Scale bars: 50 nm) of Tris-acetate solutions (5 mM) of C−Au NPs in the (a) absence and (b−d) presence of Pb^{2+} ions (1.0, 10.0, and 100 μM) at pH 7.0. The concentration of C−Au NPs was 0.24 nM. The absorbance is plotted in arbitrary units (a. u.). Inset: Photographs of C−Au NPs in the different concentrations of Pb^{2+} ions (0, 1.0, 10.0, and 100 μM).

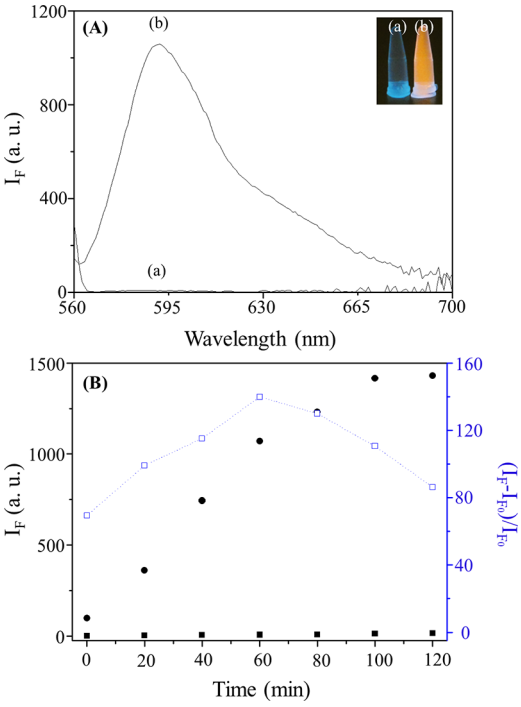

Figure 2. (A) Fluorescence spectra of Tris-acetate solutions (5 mM) of C−Au NPs in the (a) absence and (b) presence of Pb^{2+} ions (1.0 μM) at pH 7.0. The concentration of C−Au NPs was 0.24 nM. Inset: Fluorescence photographs of the H_2O_2−AUR−C−Au NP probes in the absence and presence of Pb^{2+} ions on excitation under a hand-held UV lamp (365 nm). (B) Plots of the time dependent signal enhancements (□: $(I_F - I_{F0})/I_{F0}$) and fluorescence intensity in the absence (■) and presence (●) of Pb^{2+} ions (1.0 μM).

Scheme 2. Possible Reaction Mechanism

$$C\text{–}Au^0 + Pb^{2+} \rightarrow Pb^{2+}\text{–}C\text{–}Au^0 \text{ (or } Pb\text{–}C\text{–}Au^{2+}) \quad (1)$$

$$Pb^{2+}\text{–}C\text{–}Au^0 \text{ (or } Pb\text{–}C\text{–}Au^{2+}) + 2H_2O_2 + AUR \rightarrow Pb\text{–}C\text{–}Au^0 + AUR \text{ product} + 2H_2O + O_2 \quad (2)$$

has been shown that the SPR band position and intensity are mainly determined by the morphology of the particles. It is important to note that catechin acts as a reducing and capping agent for reducing $AuCl_4^-$ ions and stabilizing the as-prepared spherical Au NPs.[31,32] When the concentration of the catechin was 0.2 mM, the size of C−Au NPs was 48.1 ± 9.5 nm, as indicated in the TEM image (see (c) in Figure S1B, Supporting Information). At the catechin concentration of 0.6 mM, the spherical C−Au NPs underwent anisotropic growth to form star-like C−Au NPs, as can be seen in the TEM images (see (d) in Figure S1B, Supporting Information). At 1.0 and 1.4 mM catechin, irregular C−Au nanostructures were formed, as depicted in the TEM images (see (e) and (f) in Figure S1B, Supporting Information) with sizes of 39.2 ± 9.8 and 27.5 ±

Table 1. Hydrodynamic Diameter, Zeta Potential, and AAS-Based Quantitation of the Pb Atoms on the C−Au NPs in the Presence of Various Concentrations of Pb^{2+} Ions

	C−Au NPs		
added Pb^{2+} (μM)	hydrodynamic diameter (nm)	zeta potential (mV)	AAS-based quantitation of the Pb atoms on the C−Au NPs (Pb atoms/C−Au NP)
0	49.6	−32.7	0
1.0	56.8	−31.6	597
10.0	54.5	−29.3	6746
100.0	122.9	−24.6	23460

dx.doi.org/10.1021/am3030454 | ACS Appl. Mater. Interfaces 2013, 5, 1503−1509

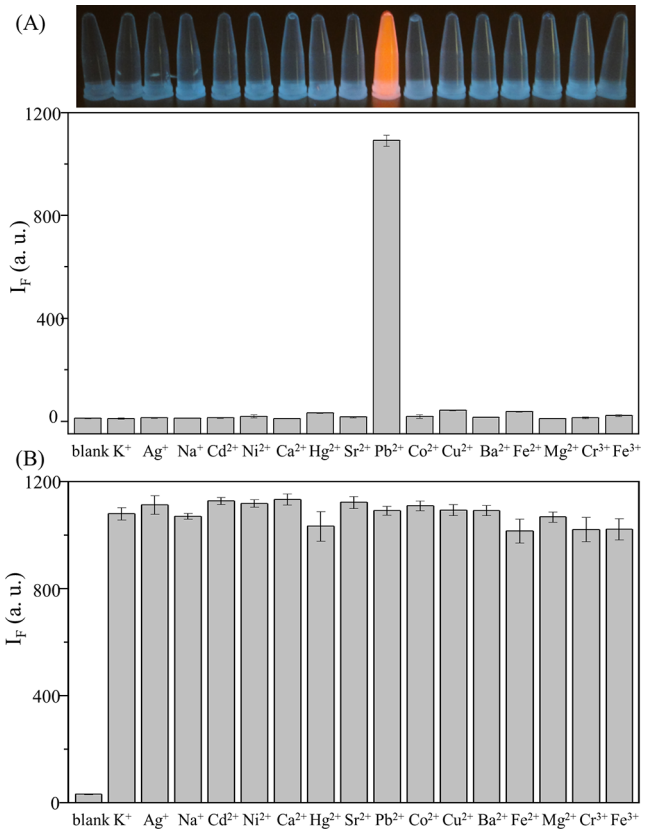

Figure 3. (A) Selectivity of the H_2O_2–AUR–C–Au NP probe toward Pb^{2+} ions (n = 3). Fluorescence photographs of the H_2O_2–AUR–C–Au NP probe with different metal ions on excitation under a hand-held UV lamp (365 nm). The concentration of Pb^{2+} ions was 1.0 μM, and the concentration of each of the other metal ions was 10 μM. (B) Tolerance of the H_2O_2–AUR–C–Au NP probe in the presence of Pb^{2+} ions (1.0 μM) and various metal ions (n = 3). The concentrations of K^+, Ag^+, Na^+, Cd^{2+}, Ni^{2+}, Ca^{2+}, Sr^{2+}, Co^{2+}, Cu^{2+}, Ba^{2+}, and Mg^{2+} ions were 100 μM, and those of Hg^{2+}, Fe^{2+}, Cr^{3+}, and Fe^{3+} ions were 10 μM.

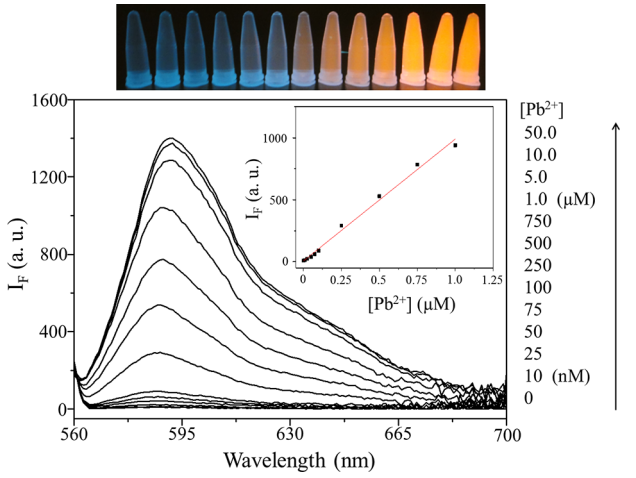

Figure 4. Fluorescence spectra and linear responses (inset) of the fluorescence intensity plotted with respect to the concentration of Pb^{2+} ions. Fluorescence photographs of the H_2O_2–AUR–C–Au NP probe with respect to the concentration of Pb^{2+} ions on excitation under a hand-held UV lamp (365 nm).

Table 2. Determination of Pb^{2+} Ions in Lake and Pond Water Using the Standard Addition Method (n = 3)

method	samples	
	lake water	pond water
	Pb^{2+} Concentration (μgL^{-1})	
current assay	4.89 ± 1.10	3.14 ± 1.05
AAS	3.66 ± 0.30	2.20 ± 0.36

11.9 nm, respectively. Upon increasing the concentration of the reducing agents, nucleation rather than particle growth controlled the formation of Au NPs. As a result, small Au NPs (5–15 nm) were formed. The EDS spectrum of C–Au NPs (see Figure S2A, Supporting Information) confirmed the existence of Au atoms. The crystal structure and phase composition of C–Au NPs were further characterized by XRD (see Figure S2B, Supporting Information). Five peaks at 2θ = 38.1°, 44.3°, 64.5°, 77.5°, and 81.7° corresponded to the diffractions from the (111), (200), (220), (311), and (222) lattice planes, respectively, of face centered cubic Au, revealing the existence of pure crystalline Au structures.

To prove that catechin acts as a capping agent for stabilization of the as-prepared C–Au NPs, FT-IR and SALDI-MS experiments were also performed for the as-prepared C–Au NPs using 0.2 mM catechin. The FT-IR spectra of (a) catechin and (b) C–Au NPs were illustrated in Figure S3A, Supporting Information. The catechin exhibited an O–H stretching band at approximately 3400 cm^{-1}, a C=O stretching band at approximately 1689 cm^{-1}, an aromatic C–C stretching band at approximately 1604 cm^{-1}, and C–O stretching bands at 1037, 1145, and 1234 cm^{-1}. Comparison of this spectrum with the FT-IR spectrum of C–Au NPs revealed the existence of catechin on the surface of C–Au NPs. The different transmittance values for the two samples are mainly because of the different concentrations of catechin on the surface of C–Au NPs. Figure S3B, Supporting Information, presented the SALDI-MS spectra of catechin and C–Au NPs. The signals at m/z 288.992 were assigned to $[\text{catechin} - H]^-$. These results further confirmed that catechin plays an essential role in stabilizing the as-prepared C–Au NPs.

Analysis of Pb^{2+} Using C–Au NPs. Recent studies have shown that the protective effect of tea catechins on PC12 cells exposed to Pb might be relative to their scavenging ability for free radicals and their chelating ability with Pb^{2+} ions.[33] Therefore, the practicality of the use of C–Au NPs for sensing Pb^{2+} ions was evaluated. Scheme 1 displayed the sensing strategy of C–Au NPs toward Pb^{2+} ions. C–Au NPs reacted with Pb^{2+} ions at pH 7.0 to form Pb–catechin complexes and Pb–Au alloys on their surfaces, which increased catalytic activity of the modified C–Au NPs for the H_2O_2-mediated oxidation of AUR. Although AUR itself is weakly fluorescent, its oxidation product is highly fluorescent [quantum yield (Φ): 70%].[34,35] As a result, the fluorescence of the solutions at 588 nm increased when they were excited at 540 nm. In contrast, 32 and 56 nm Au NPs synthesized by sodium citrate and Pb^{2+} ions have negligible catalytic activity toward the H_2O_2-mediated oxidation of AUR at pH 7.0.

The absorption spectra of C–Au NPs (0.24 nM) prepared using 0.2 mM catechin in Tris-acetate (5 mM, pH 7.0) in the absence and presence of Pb^{2+} ions (1.0 and 10.0 μM) for 60 min revealed similar maximum absorption wavelengths of the SPR bands (Figure 1a–c). Although partial Tris cations existed at pH 7.0, catechin molecules on the surface of Au NPs

Table 3. Non-DNA Functionalized Au NP-Based Optical Methods for the Determination of Pb^{2+} Ions

method	probe	analytical ranges/LODs	real sample	ref.
fluorescence	glutathione-Au NDs	5 nM−5 μM/2 nM	lake water	47
	Au NPs	5.0 nM−1.0 μM/4 nM	pond water and blood samples	30
colorimetric	glutathione/pentapeptides (CALNN)-Au NPs	1−5 μM/1 μM	HeLa cells	48
	BSA-Au NPs/thiosulfate and 2-mercaptoethanol	10 nM−1.0 μM/5 nM	seawater, urine, and blood samples	49
	gallic acid-Au NPs	10−800 nM/10 nM	drinking water	50
	CALNN-Au NPs	0.1−30 μM/0.1 μM	−[a]	51
	azacrown ether- Au NPs	−[a]/0.1 mM	−[a]	52
	glutathione-Au NPs	0.1−50 μM/100 nM	lake water	53
	2-mercaptoethanol-Au NPs	50−500 nM/45 nM	river water and Montana soil samples	54
	4-mercaptobutanol/thiosulfate-Au NPs	0.5−10 nM/0.2 nM	Montana soil and urine samples	55
	gallic acid-Au NPs	0.5 nM−1.0 μM/0.25 nM	drinking water	56
	glycine-Au NPs	2−30 μM/5 μM	−[a]	57
fluorescence	catechin-Au NPs/AUR and H_2O_2	10 nM−1.0 μM/1.5 nM	lake, pond water, and urine samples	this study

[a]Not provided.

generated steric effects. Thus, C−Au NPs were stable at pH 7.0 in either the absence or presence of Pb^{2+} ions (1.0 and 10.0 μM). The slight decrease in the SPR band in the presence of Pb^{2+} ions was due to the change in the refractive index and composition of the Au NP surfaces, as confirmed by TEM analysis. The TEM images in Figure 1B(b,c) reveal that C−Au NPs in the presence of Pb^{2+} ions (1.0 and 10.0 μM) almost remained the same sizes and shapes relative to that (Figure 1B(a)) in the absence of Pb^{2+} ions. The average sizes of C−Au NPs in the presence of 1.0 and 10.0 μM Pb^{2+} ions were 52.0 ± 5.9 and 54.8 ± 7.4 nm, respectively. Upon addition of 100 μM Pb^{2+} to C−Au NPs, the solution turned purple owing to the formation of PbO likely inducing the serious aggregation of C−Au NPs further supported by the TEM image (Figure 1B(d)), along with broadening and shifting of the SPR band (Figure 1A(d)). A Zetasizer Nano ZS90 apparatus and AAS were also employed to confirm the presence of Pb species on the C−Au NPs surfaces that had been exposed to Pb^{2+} ions (0, 1.0, 10.0, and 100 μM) at pH 7.0. Table 1 shows that the hydrodynamic diameter of C−Au NPs slightly increased, and the zeta potentials of C−Au NPs moved toward a less negative charge when Pb^{2+} ion concentration increased from 0 to 10.0 μM. These results suggested the possible existence of Pb−catechin complexes on the C−Au NP surfaces. We also noted that the hydroxyl groups of catechins acting as the electron donors led to ease in the formation of Pb−Au alloys. At high concentration of Pb^{2+} ions (100 μM), the hydrodynamic diameter of C−Au NPs increased to 122.9 nm and the zeta potentials moved toward a least negative charge (−24.6 mV), resulting in the serious aggregation of C−Au NPs. To confirm this assumption, AAS was used to quantify the Pb atoms obtained from each C−Au NP after a series of centrifugation/washing steps for removal of any unbound species. The depositions of Pb atoms on each C−Au NP also increased as the concentration of Pb^{2+} ions increased. Considering the mechanism shown in Scheme 1, it is highly possible that Pb−catechin complexes and Pb−Au alloys exist on the C−Au NPs surface.

Figure 2A reveals that C−Au NPs in the presence of Pb^{2+} ions had great catalytic activity at pH 7.0 than they did in the absence of the metal ions. It is difficult to oxidize AUR at low pH values. At the values of pH greater than 7.0, Pb^{2+} ions form various species, such as PbO, through reactions with OH^- ions, thereby minimizing the formation of Pb−catechin complexes or Pb−Au alloys (Figure S4, Supporting Information). The generation of fluorescence was also measured as a function of time. As shown in Figure 2B, the fluorescence signal gently increased from 0 to 100 min, remaining constant thereafter. Simultaneously, the background noise increased with time. The optimal S/N ratio was observed at an incubation time of 60 min. Therefore, reactions were incubated for 60 min at room temperature in all of the assays.

The binding energies (BEs) of the Au $4f_{7/2}$ electrons in the Au NPs in the absence and presence of Pb^{2+} ions were 83.0 and 84.3 eV, respectively, while $4f_{5/2}$ electrons in the C−Au NPs in the absence and presence of Pb^{2+} ions they were 86.6 and 87.9 eV, respectively (Figure S5A, Supporting Information). Thus, the metal ions induced increase in the oxidation states of the C−Au NPs surfaces.[36] The BEs of the Pb $4f_{7/2}$ and $4f_{5/2}$ electrons were 139.6 and 144.4 eV, respectively (Figure S5B, Supporting Information), revealing the existence of ionic Pb species.[36] It has been known that metal ions catalyze the reactions of H_2O_2 with some organic compounds such as AUR and luminol.[34,37,38] The Au^{3+}/Au^{1+} on the C−Au NPs surfaces catalyze several reactions, including CO oxidation, hydrochlorination of ethyne, and the water gas shift reaction.[39−41] In our case, the high concentrations of Pb^{2+} ions and high active sites of Pb−catechin complexes on the Au NPs surfaces played significant roles in determining their catalytic activity.[42] Scheme 2 presents a possible reaction process of AUR (OH group) with H_2O_2 to form AUR product (C═O) on the surfaces of C−Au NPs.

Optimization of the Assay. Additional assay parameters were evaluated to further optimize the experimental protocol. The effect of the catechin concentration used to form C−Au NPs was tested over a range of 0.05−1.4 mM (Figure S6, Supporting Information), and it was observed that the fluorescence intensity of the AUR oxidation products increased with the concentrations of catechin up to 0.2 mM, above which it slightly decreased. This trend was probably because of the fact that Pb^{2+} ions form stable complexes with catechin on the C−Au NPs surface, resulting in increased catalytic activity of C−Au NPs in the H_2O_2-mediated oxidation of AUR. To confirm this hypothesis, AAS was again used to quantify the Pb atoms obtained from each C−Au NPs after a series of centrifugation/washing steps to remove any unbound Pb^{2+} ions. The trend in the deposition of Pb atoms on the C−Au NPs was consistent with that observed for the fluorescence results. Therefore, 0.2 mM catechin was selected as the optimal concentration for further investigations. Different concentrations of C−Au NPs ranging from 0.03 to 1.2 nM (Figure S4,

Supporting Information) were also tested, and it was found that the fluorescence intensity of the AUR oxidation product increased with increasing the C−Au NPs concentration up to 0.24 nM, above which it decreased. This result is probably because of the inner filter effects of C−Au NPs at high concentration levels. Therefore, 0.24 nM was chosen as the optimal C−Au NPs concentration in the present study.

To test the effect of the buffer system, different buffer systems including Tris-acetate, borate, phosphate, and ammonia-acetate buffers were considered. As can be seen in Figure S7A, Supporting Information, the maximum fluorescence intensity for Pb^{2+} ion detection was obtained when Tris-acetate buffer was used. The hydroxyl groups of Tris acting as the electron donors led to ease in the formation of Pb−Au alloys, resulting in greater catalytic efficiency. Therefore, Tris-acetate buffer system was selected for further study. In addition, the influences of the Tris-acetate buffer concentrations in the range from 2.0 to 35 mM were tested (Figure S7B, Supporting Information). The fluorescence intensity of the AUR oxidation product increased with an increase in the concentration of the Tris-acetate buffer up to 5.0 mM, above which the fluorescence intensity decreased. Therefore, 5.0 mM Tris-acetate was selected as the optimal condition for further investigations.

The effect of the hydrogen peroxide concentration was tested for concentrations ranging from 0 to 500 μM. For Pb^{2+} ion detection, the fluorescence intensity of the AUR oxidation product increased as the concentration of hydrogen peroxide increased up to 400 μM (Figure S8A, Supporting Information). The effect of the AUR concentration was also investigated in the range from 0 to 35 μM. In this case, the fluorescence intensity of the AUR oxidation product increased as the AUR concentration increased up to 20 μM, above which it decreased (Figure S8B, Supporting Information), probably because of the inner filter effects of the AUR at high concentration levels. Therefore, 20 μM AUR was chosen as the optimal AUR concentration in the present study.

Validation of the Assay. To investigate the selectivity of the C−Au NPs probe toward Pb^{2+} ions, Pb^{2+} (1.0 μM), K^+, Ag^+, Na^+, Cd^{2+}, Ni^{2+}, Ca^{2+}, Hg^{2+}, Sr^{2+}, Co^{2+}, Cu^{2+}, Ba^{2+}, Fe^{2+}, Mg^{2+}, Cr^{3+}, and Fe^{3+} ions (each at a concentration of 10 μM) were added to the C−Au NPs probe (one additional ion at a time) in the presence of the AUR-hydrogen peroxide solution. At pH 7.0, only Pb^{2+} ions induced significant increases in the fluorescence (i.e., formed the AUR oxidation product) (Figure 3A). To further test the practicality of the H_2O_2−AUR−C−Au NP probe, we conducted fluorescent measurements in mixtures containing Pb^{2+} (1.0 μM) and possible interference ions such as K^+, Ag^+, Na^+, Cd^{2+}, Ni^{2+}, Ca^{2+}, Sr^{2+}, Co^{2+}, Cu^{2+}, Ba^{2+}, and Mg^{2+} ions (each at a concentration of 100 μM) and Hg^{2+}, Fe^{2+}, Cr^{3+} and Fe^{3+} ions (each at a concentration of 10 μM). The resulting data (Figure 3B) demonstrated that the high selectivity of the H_2O_2−AUR−C−Au NP probe toward Pb^{2+} ions in the presence of other metal ions still counted. These results suggested that this detection system might be practical for the quantitative detection of Pb^{2+} ions in environmental samples.

Under the optimal conditions, the sensitivity of the C−Au NPs probe toward Pb^{2+} ions was then investigated. The fluorescence intensity of the AUR oxidation product increased with increasing the concentration of Pb^{2+} ions up to 50 μM, above which it decreased (data not shown), because of the aggregation of C−Au NPs. Although the obvious change in fluorescence of H_2O_2−AUR−C−Au NP is limited when the concentration of Pb^{2+} ranged from 10 to 250 nM, a linear relationship was obtained from the plot of fluorescence intensity as a function of the concentration of Pb^{2+} ions over the range of 10 nM−1.0 μM (R^2 = 0.99) (Figure 4). The C−Au NPs probe to detect Pb^{2+} ions exhibited a limit of detection (S/N = 3) of 1.5 nM, which is well below the maximum level of Pb^{2+} ions permitted by the U.S. EPA for drinking water (72 nM; 15 μgL^{-1}). This value is comparable with what (1.0 nM) we determined previously using a G-quadruplex DNAzyme.[14] Relative to DNAzyme, C−Au NPs are easier to synthesize, less expensive, and more stable. Moreover, detection time only requires 1 h at ambient temperature due to greater catalytic efficiency of the H_2O_2−AUR−C−Au NP probe.

Application of the Assay. To test the practicality of the newly developed probe, Pb^{2+} ions in lake and pond water samples were analyzed. The C−Au NPs probe, in conjunction with a standard addition method, was used to determine the concentration of Pb^{2+} ions in lake and pond water samples (Table 2). The results of the assay were compared with the measurements obtained via AAS. Using the *F*-test (the *F* value was 19 at a 95% confidence level), the *F* values calculated at the 95% confidence level for the lake and pond water samples were 13.4 and 8.5, respectively, revealing that no significant differences existed between the precision of the new assay and the AAS method. Then, using the *t* test (the *t* test value was 2.776 at a 95% confidence level), the *t* values calculated at the 95% confidence level for the lake and pond water samples were 0.012 and 1.47, respectively. These results showed that the data obtained from the two methods were not significantly different. Linear correlations (R^2 > 0.96) were then obtained between the responses and concentrations of Pb^{2+} ion spiked into urine samples over the range of 10 nM−1.0 μM (Figure S9, Supporting Information). The recoveries of these measurements were 91.2−117.8%. The presence of Pb^{2+} ions was not detected in the urine samples using either the new detection system or AAS-based analysis. Thus, the new C−Au NPs probe is a practical tool for the determination of Pb^{2+} ions in real samples. This assay abrogates the need for the synthesis of complicated chemosensors or the use of sophisticated instruments.[43−46] In addition, in comparison to other non-DNA functionalized Au NP-based optical methods (Table 3), the new assay for Pb^{2+} ions is relatively simple (one-pot synthesis), selective, and sensitive.[30,47−57]

CONCLUSIONS

We have developed a highly sensitive and selective approach to detect Pb^{2+} ion. The formation of Pb−catechin complexes and Pb−Au alloys results in C−Au NPs exhibiting peroxidase mimicking activity, catalyzing the oxidation of AUR in the presence of hydrogen peroxide. This novel probe possesses several attractive features when compared with other reported optical approaches: (1) low cost and simplicity, expensive enzymes, DNA, and other recognition elements and sophisticated instruments (AAS, inductively coupled plasma mass spectrometry) are not required; (2) sensitivity, the LOD for Pb^{2+} ions in the neutral condition is 1.50 nM; (3) practicality, analysis of complicated samples (lake and pond water, as well as urine samples) is possible without performing tedious sample pretreatment. In addition, because the method is also dependent on the amount of hydrogen peroxide, our approach might be applicable to the detection of various substrates or activity of various enzymes when combined with enzymatic reactions.

■ ASSOCIATED CONTENT

Supporting Information

Figures S1−S9. This information is available free of charge via the Internet at http://pubs.acs.org/.

■ AUTHOR INFORMATION

Corresponding Author

*E-mail: linyejerry@cc.ncue.edu.tw.

Notes

The authors declare no competing financial interest.

■ ACKNOWLEDGMENTS

This study was supported by National Science Council of Taiwan under contracts NSC 101-2113-M-018-001-MY2 and NSC 101-2120-S-018-003. The authors would like to thank Enago (www.enago.tw) for the English language review.

■ REFERENCES

(1) Meadows-Oliver, M. *J. Pediatr. Health Care* **2012**, *26*, 213−215.
(2) Iqbal, M. P. *Pak. J. Pharm. Sci.* **2012**, *25*, 289−294.
(3) Wu, Q. L.; Liu, P. D.; Li, Y. X.; Du, M.; Xing, X. J.; Wang, D. Y. *J. Environ. Sci.-China* **2012**, *24*, 733−742.
(4) Huang, H. G.; Gupta, D. K.; Tian, S. K.; Yang, X. E.; Li, T. X. *Environ. Sci. Pollut. Res.* **2012**, *19*, 1640−1651.
(5) Olayinka, O. I.; Nta, H. A.; Ganiyat, A. *J. Med. Plants Res.* **2011**, *5*, 2743−2747.
(6) Pandya, C.; Pillai, P.; Nampoothiri, L. P.; Bhatt, N.; Gupta, S.; Gupta, S. *Andrologia* **2012**, *44*, 813−822.
(7) Sobin, C.; Parisi, N.; Schaub, T.; Gutierrez, M.; Ortega, A. X. *Arch. Environ. Contam. Toxicol.* **2011**, *61*, 521−529.
(8) Menezes, J. A.; Viana, G. F. D.; Paes, C. R. *Environ. Monit. Assess.* **2012**, *184*, 2593−2603.
(9) Eom, M. S.; Kim, S.; Seo, S. H.; Han, M. S. *Bull. Korean Chem. Soc.* **2012**, *33*, 316−318.
(10) Liu, M. Y.; Lou, X. H.; Du, J.; Guan, M.; Wang, J.; Ding, X. F.; Zhao, J. L. *Analyst* **2012**, *137*, 70−72.
(11) Li, H.; Zhang, Q.; Cai, Y.; Kong, D. M.; Shen, H. X. *Biosens. Bioelectron.* **2012**, *34*, 159−164.
(12) Guo, L. Q.; Nie, D. D.; Qiu, C. Y.; Zheng, Q. S.; Wu, H. Y.; Ye, P. R.; Hao, Y. L.; Fu, F. F.; Chen, G. N. *Biosens. Bioelectron.* **2012**, *35*, 123−127.
(13) Lin, Y. W.; Liu, C. W.; Chang, H. T. *Talanta* **2011**, *84*, 324−329.
(14) Li, C. L.; Liu, K. T.; Lin, Y. W.; Chang, H. T. *Anal. Chem.* **2011**, *83*, 225−230.
(15) Li, R. S.; Yan, H. T.; Yang, X. M.; Li, Z. X.; Guo, Y. A. *J. Anal. At. Spectrom.* **2011**, *26*, 1488−1493.
(16) Zhang, H. X.; Jiang, B. Y.; Xiang, Y.; Su, J.; Chai, Y. Q.; Yuan, R. *Biosens. Bioelectron.* **2011**, *28*, 135−138.
(17) Zhang, L. B.; Han, B. Y.; Li, T.; Wang, E. K. *Chem. Commun.* **2011**, *47*, 3099−3101.
(18) Li, T.; Dong, S. J.; Wang, E. K. *J. Am. Chem. Soc.* **2010**, *132*, 13156−13157.
(19) Zhang, X. B.; Wang, Z. D.; Xing, H.; Xiang, Y.; Lu, Y. *Anal. Chem.* **2010**, *82*, 5005−5011.
(20) Ito, Y.; Fukusaki, E. *J. Mol. Catal. B: Enzym.* **2004**, *28*, 155−166.
(21) Saha, K.; Agasti, S. S.; Kim, C.; Li, X. N.; Rotello, V. M. *Chem. Rev.* **2012**, *112*, 2739−2779.
(22) Fu, X. L.; Lou, T. T.; Chen, Z. P.; Lin, M.; Feng, W. W.; Chen, L. X. *ACS Appl. Mater. Interfaces* **2012**, *4*, 1080−1086.
(23) Lou, T. T.; Chen, Z. P.; Wang, Y. Q.; Chen, L. X. *ACS Appl. Mater. Interfaces* **2011**, *3*, 1568−1573.
(24) Lou, T. T.; Chen, L. X.; Chen, Z. P.; Wang, Y. Q.; Chen, L.; Li, J. H. *ACS Appl. Mater. Interfaces* **2011**, *3*, 4215−4220.
(25) Xu, H.; Liu, B. X.; Chen, Y. *Microchim. Acta* **2012**, *177*, 89−94.
(26) Lin, Y. W.; Huang, C. C.; Chang, H. T. *Analyst* **2011**, *136*, 863−871.
(27) Knecht, M. R.; Sethi, M. *Anal. Bioanal. Chem.* **2009**, *394*, 33−46.
(28) Wang, Z. D.; Lee, J. H.; Lu, Y. *Adv. Mater.* **2008**, *20*, 3263−3267.
(29) Wei, H.; Li, B. L.; Li, J.; Dong, S. J.; Wang, E. K. *Nanotechnology* **2008**, *19*, 095501−095505.
(30) Wang, C. I.; Huang, C. C.; Lin, Y. W.; Chen, W. T.; Chang, H. T. *Anal. Chim. Acta* **2012**, *745*, 124−130.
(31) Kamal, S. S. K.; Sahoo, P. K.; Premkumar, M.; Sreedhar, B.; Ram, S. *Adv. Sci. Lett.* **2010**, *3*, 144−148.
(32) Begum, N. A.; Mondal, S.; Basu, S.; Laskar, R. A.; Mandal, D. *Colloids Surf., B* **2009**, *71*, 113−118.
(33) Chen, L.; Yang, X. Q.; Jiao, H.; Zhao, B. *Chem. Res. Toxicol.* **2004**, *17*, 922−928.
(34) Liu, C. H.; Tseng, W. L. *Anal. Chim. Acta* **2011**, *703*, 87−93.
(35) Zhu, A. P.; Romero, R.; Petty, H. R. *Anal. Biochem.* **2010**, *403*, 123−125.
(36) Chen, Y. Y.; Chang, H. T.; Shiang, Y. C.; Hung, Y. L.; Chiang, C. K.; Huang, C. C. *Anal. Chem.* **2009**, *81*, 9433−9439.
(37) Liu, C. H.; Yu, C. J.; Tseng, W. L. *Anal. Chim. Acta* **2012**, *745*, 143−148.
(38) Wang, C. I.; Chen, W. T.; Chang, H. T. *Anal. Chem.* **2012**, *84*, 9706−9712.
(39) Hodge, N.; Kiely, C.; Whyman, R.; Siddiqui, M.; Hutchings, G.; Pankhurst, Q.; Wagner, F.; Rajaram, R.; Golunski, S. *Catal. Today* **2002**, *72*, 133−144.
(40) Nkosi, B.; Coville, N. J.; Hutchings, G. J.; Adams, M. D.; Friedl, J.; Wagner, F. E. *J. Catal.* **1991**, *128*, 366−377.
(41) Fu, Q.; Saltsburg, H.; Flytzani-Stephanopoulos, M. *Science* **2003**, *301*, 935−938.
(42) Xie, J. X.; Zhang, X. D.; Wang, H.; Zheng, H. Z.; Huang, Y. M. *TrAC, Trends Anal. Chem.* **2012**, *39*, 114−129.
(43) Kim, H. N.; Ren, W. X.; Kim, J. S.; Yoon, J. *Chem. Soc. Rev.* **2012**, *41*, 3210−3244.
(44) LLerena, F.; Maynar, M.; Barrientos, G.; Palomo, R.; Robles, M. C.; Caballero, M. J. *Eur. J. Appl. Physiol.* **2012**, *112*, 3027−3031.
(45) Kruger, P. C.; Bloom, M. S.; Arnason, J. G.; Palmer, C. D.; Fujimoto, V. Y.; Parsons, P. J. *J. Anal. At. Spectrom.* **2012**, *27*, 1245−1253.
(46) Trujillo, I. S.; Alonso, E. V.; de Torres, A. G.; Pavon, J. M. C. *Microchem. J.* **2012**, *101*, 87−94.
(47) Yuan, Z. Q.; Peng, M. H.; He, Y.; Yeung, E. S. *Chem. Commun.* **2011**, *47*, 11981−11983.
(48) Zhu, D. R.; Li, X. K.; Liu, X.; Wang, J. N.; Wang, Z. X. *Biosens. Bioelectron.* **2012**, *31*, 505−509.
(49) Lee, Y. F.; Huang, C. C. *ACS Appl. Mater. Interfaces* **2011**, *3*, 2747−2754.
(50) Huang, K. W.; Yu, C. J.; Tseng, W. L. *Biosens. Bioelectron.* **2010**, *25*, 984−989.
(51) Li, X. K.; Wang, Z. X. *Chem. Res. Chin. Univ.* **2010**, *26*, 194−197.
(52) Alizadeh, A.; Khodaei, M. M.; Karami, C.; Workentin, M. S.; Shamsipur, M.; Sadeghi, M. *Nanotechnology* **2010**, *21*, 315503−315510.
(53) Chai, F.; Wang, C. A.; Wang, T. T.; Li, L.; Su, Z. M. *ACS Appl. Mater. Interfaces* **2010**, *2*, 1466−1470.
(54) Hung, Y. L.; Hsiung, T. M.; Chen, Y. Y.; Huang, Y. F.; Huang, C. C. *J. Phys. Chem. C* **2010**, *114*, 16329−16334.
(55) Hung, Y. L.; Hsiung, T. M.; Chen, Y. Y.; Huang, C. C. *Talanta* **2010**, *82*, 516−522.
(56) Ding, N.; Cao, Q. A.; Zhao, H.; Yang, Y. M.; Zeng, L. X.; He, Y. J.; Xiang, K. X.; Wang, G. W. *Sensors-Basel* **2010**, *10*, 11144−11155.
(57) Hamaguchi, K.; Kawasaki, H.; Arakawa, R. *Colloids Surf., A* **2010**, *367*, 167−173.